materials

MDPI

Article

Preparation of $LiFePO_4$ Powders by Ultrasonic Spray Drying Method and Their Memory Effect

Tu Lan [1], Xiaolong Guo [1,*], De Li [1,*] and Yong Chen [1,2,*]

[1] State Key Laboratory on Marine Resource Utilization in South China Sea, Hainan Provincial Key Laboratory of Research on Utilization of Si-Zr-Ti Resources, School of Materials Science and Engineering, Hainan University, Haikou 570228, China; 18085204210017@hainanu.edu.cn

[2] Guangdong Key Laboratory for Hydrogen Energy Technologies, School of Materials Science and Hydrogen Energy, Foshan University, Foshan 528000, China

* Correspondence: xiaolongaca@163.com (X.G.); lidenju@sina.com (D.L.); ychen2002@163.com (Y.C.)

Abstract: The memory effect of lithium-ion batteries (LIBs) was first discovered in $LiFePO_4$, but its origin and dependence are still not clear, which is essential for regulating the memory effect. In this paper, a home-made spray drying device was used to successfully synthesize $LiFePO_4$ with an average particle size of about 1 μm, and we studied the influence of spray drying temperature on the memory effect of $LiFePO_4$ in LIBs. The results showed that the increasing of spray drying temperature made the memory effect of $LiFePO_4$ strengthen from 1.3 mV to 2.9 mV, while the capacity decreased by approximately 6%. The XRD refinement and FTIR spectra indicate that the enhancement of memory effect can be attributed to the increment of Li–Fe dislocations. This work reveals the dependence of memory effect of $LiFePO_4$ on spray drying temperature, which will guide us to optimize the preparation process of electrode materials and improve the management system of LIBs.

Keywords: $LiFePO_4$; spray drying method; memory effect; cathode materials

Citation: Lan, T.; Guo, X.; Li, D.; Chen, Y. Preparation of $LiFePO_4$ Powders by Ultrasonic Spray Drying Method and Their Memory Effect. *Materials* **2021**, *14*, 3193. https://doi.org/10.3390/ma14123193

Academic Editor: Alessandro Dell'Era

Received: 8 May 2021
Accepted: 3 June 2021
Published: 10 June 2021

1. Introduction

Due to energy shortage and environmental pollution, lithium-ion batteries (LIBs) have attracted enormous attention for their high energy density, long service life, and excellent safety performance [1–4]. With the development of science and technology, LIBs exhibit a lot of applications, which require superior performances [5–7]. As an important component of LIBs, the cathode material directly affects the electrochemical performance of LIBs [8–11]. Olivine-type $LiFePO_4$, which has a high theoretical specific capacity of 170 mAh/g, excellent thermal stability, environmental friendliness and low price, is considered to be a promising cathode material for LIBs [12,13]. The research on $LiFePO_4$ mainly focuses on electronic conductive coating [14,15], ion doping [16,17], particle size optimization [18,19], such as reducing the particle size of $LiFePO_4$ to overcome weak ionic conductivity, using carbon coating on active particles to improve electronic conductivity.

$LiFePO_4$ is usually synthesized by high-temperature solid-phase method, liquid-phase method, coprecipitation method, microwave heating and other methods [20–23]. High-temperature solid-state method is widely used and realizes industrial production due to its simple process, easy control of preparation conditions. However, the prepared electrode materials have the disadvantages of irregular particle shape, large grain size, unstable electrochemical performance, etc. Wet chemical methods, such as sol–gel method, hydrothermal method and coprecipitation method, can mix raw materials at molecular level with low temperature [24,25]. The prepared cathode materials have good conductivity, small particle size and uniform distribution, but high cost severely limits the output. The spray drying method, a method for atomizing the precursor solution into fine mist droplets, and then instantly drying them to solid particles in a high-temperature environment,

has been widely used to prepare spherical micro powder in food, medicine, electronics, materials and other fields [26]. This method can achieve continuous production, and the prepared material particles have high purity and uniform and controllable size [27–31].

Eight years ago, Sasaki et al. [32] first discovered the memory effect of $LiFePO_4$ in LIBs, which was also found in other two-phase materials later [33,34]. The memory effect refers to the fact that the battery memorizes the history of charge and discharge, and it can affect the battery performance, such as reducing the specific capacity and the service time [35]. As a voltage bump or step during the charging and discharging plateau, the memory effect can delay the two-phase transition, affect the estimation of the state of charge (SOC) and reduce the energy efficiency of LIBs [36,37]. In recent years, the memory effect of LIBs has been investigated from virous aspects, such as the relaxation time after phase transition and sintering temperature [37], particle size [36], ion doping [34], memory writing process [38], lithium excess [39], and oxygen vacancies [40].

In our previous work, the memory effect of $LiFePO_4$ was obviously dependent on the relaxation time after the phase transition, of which the voltage bump was actually a delayed voltage overshooting [37], and it is also affected by the particle size of $LiFePO_4$ [36]. Although the sintering temperature was proved to affect the memory effect of $LiFePO_4$ [37], there is no report about the influence of spray drying temperature on the memory effect. In this work, a series of $LiFePO_4$ samples were prepared by using home-made spray drying equipment, characterized by TGA analysis, SEM images, XRD refinement and FTIR spectra, in order to study the influence of spray drying temperature on the memory effect.

2. Materials and Methods

2.1. Preparation of $LiFePO_4$ by Spray Drying Method

First, 0.036 mol LiH_2PO_4 (99.9%, Aladdin, Shanghai, China), 0.036 mol $FeCl_2 \cdot 4H_2O$ (99.9%, Aladdin, Shanghai, China), 0.00108 mol $LiOH \cdot H_2O$ (99.9%, Aladdin, Shanghai, China), 15 mL hydrochloric acid (36–38%, Xilong Chemical, Guangzhou, China) and 0.85188 g sucrose (99.9%, Aladdin, Shanghai, China) were successively added into 50 mL deionized water, diluted to 200 mL and the precursor solution was obtained after thorough stirring. The precursor solution was atomized by the ultrasonic atomizer (402AI, Yuewell Company, Suzhou, China) at a frequency of 1.7 MHz, and then brought into a tube furnace (BTF-1100C-S, Anhui Bei Keke Equipment Technology Co., Ltd., Anhui, China) by 5% H_2/Ar at various temperatures (200 °C, 250 °C, 300 °C and 350 °C, respectively) after the negative ion generator was turned on. Before this process, the air in the tube furnace was replaced with 5 L/min of 5% H_2/Ar for 15 min. After spray drying, the $LiFePO_4$ precursor powder was ground for 1 h and placed into the tube furnace. Under the 5% H_2/Ar atmosphere, the furnace temperature was raised to 650 °C at a heating rate of 10 °C/min and kept for 8 h. The $LiFePO_4$ samples were collected after naturally cooling to room temperature.

2.2. Characterization of Materials

D2 PHASER with filtered Cu Kα radiation, produced by Bruker company of Germany, was used to test the X-ray diffractometer (XRD, Bruker D8 advance, Bruker, Karlsruhe, Germany). The high-quality XRD patterns were collected by step scanning with the scanning range of 10° to 80° and a step width of 0.01° at room temperature. The Rietveld refinement was carried out by the General Structure Analysis System (GSAS 1.00, Regents of the University of California, CA, USA) with the EXPGUI interface [41]. The refinement process is as follows: the background and scale factor parameters are firstly determined; the scale factor is refined and 20 background coefficients are used for the Chebyshev polynomial function; the following instrumental/structural parameters, zero-shift, lattice parameters and profile parameters are refined. The thermal analysis was conducted on Q600SDT (TA Instruments, New Castle, DE, USA) at a heating rate of 10 °C min^{-1} from room temperature to 850 °C with an air flow of 20 mL/min. FTIR spectra were collected on PerkinElmer FTIR Spectrometer (FTIR, Perkin-Elmer Frontier, Perkin-ElmER, Waltham,

MA, USA) with a resolution of 1 cm^{-1}. Then, the morphology of as-prepared $LiFePO_4$ precursor powders were characterized by scanning electron microscope (SEM, Phenom ProX, Phenom-World BV, Eindhoven, Netherlands).

2.3. Electrochemical Characterization

$LiFePO_4$, acetylene black and binder PTFE were mixed with a mass ratio of 42.5:42.5:15 and rolled into a film. The film was cut into a disc with a diameter of 10 mm and pressed evenly on an aluminum mesh, dried at 80 °C for 12 h in a vacuum drying oven, and the cathode was prepared. The $LiFePO_4$ film, lithium metal and Celgard 2400 microporous polypropylene film are positive electrode, negative electrode and separator respectively, and the electrolyte is 1 mol/L $LiClO_4$/EC + DEC (volume ratio 1:1). The CR2025 button cell was assembled in a glove box and tested after rest for 12 h. The galvanostatic current charge/discharge test was carried out in the voltage range of 2.8 V to 4.0 V at 25 °C by the Hokuto Denko battery test system (HJ1001SD8, Hokuto Denko Corporation, Gifu, Japan).

3. Results and Discussion

Figure 1 is a schematic diagram of a home-made spray drying device, which mainly consists of an ultrasonic atomizer, a tubular furnace, a negative ion generator and an air outlet pipe. Before starting the spray experiment, the airtightness of the device was confirmed to be in good condition. The air in the device was evacuated by introducing 5 L/min of 5% H_2/Ar gas for 15 min. The nebulizer and negative ion generator were turned on at the same time, the precursor solution was atomized into fog droplets with an average particle diameter of 3.9 microns. The fog droplets were be carried into the inclined tubular furnace by 0.5 L/min of 5% H_2/Ar gas. The fog droplets were quickly dried in contact with the high-temperature gas in the tube furnace to form solid particles. The gas in the tube furnace was partially ionized by the generator to generate negative ions, in which the solid particles tend to adsorb and deposit on the negative ion generator and the inner surface of the tube furnace. Then the gas was vented from the exhaust pipe. In this work, we adjusted the temperature in the tube furnace (200 °C, 250 °C, 300 °C, 350 °C) to study the influence of spray drying temperature on the memory effect of as-synthesized $LiFePO_4$ samples.

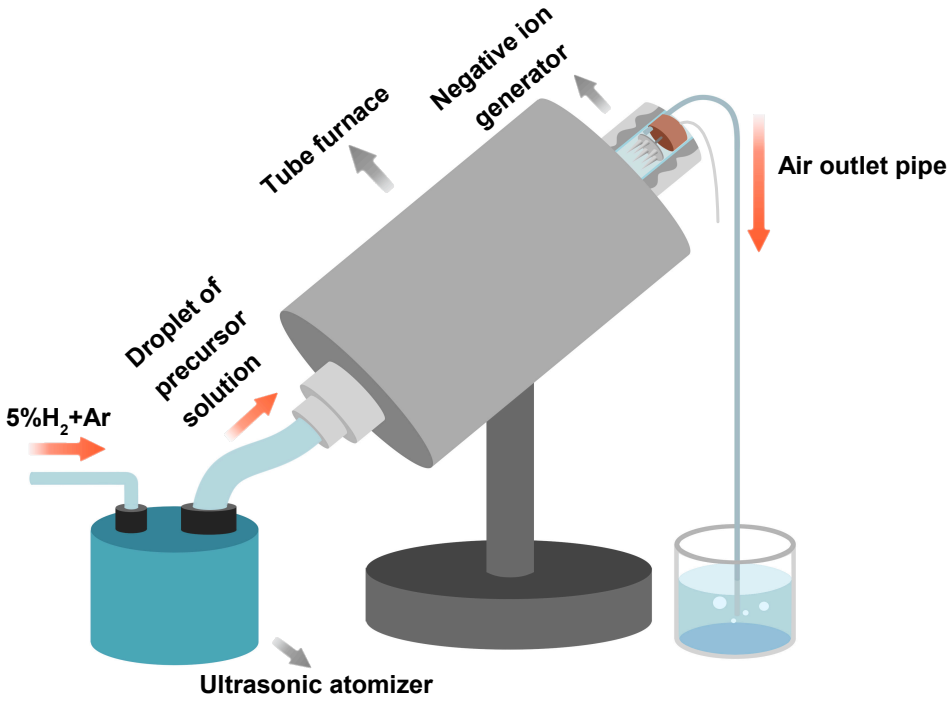

Figure 1. Schematic diagram of home-made spray drying device.

Figure 2 presents SEM photos of as-synthesized $LiFePO_4$ precursor powder prepared at spray drying temperature of 200 °C, 250 °C, 300 °C and 350 °C, respectively. SEM images show that the $LiFePO_4$ precursor particles are mainly spherical. Figure 3 shows the particle size analysis results of four temperatures, in which the particle size is mainly between 0.4 μm and 1.2 μm, accounting for more than 85%. The $LiFePO_4$ precursor of 300 °C and 350 °C have a small number of particles with a diameter of more than 1.8 μm, while such particles are virtually absent for 200 °C and 250 °C. In addition, the average particle size for 200 °C, 250 °C and 300 °C is very close at 0.79 μm, 0.77 μm and 0.78 μm, respectively, while the average particle size for 350 °C is slightly larger as 0.88 μm. The precursor particle size in this work is concentrated below 1 micron, while the precursor particle size prepared by Yu F et al. is far greater than 1 micron [37,42]. In fact, the ultrasonic atomization method that we used can produce a smaller particle size, resulting in better electrochemical performance [43,44].

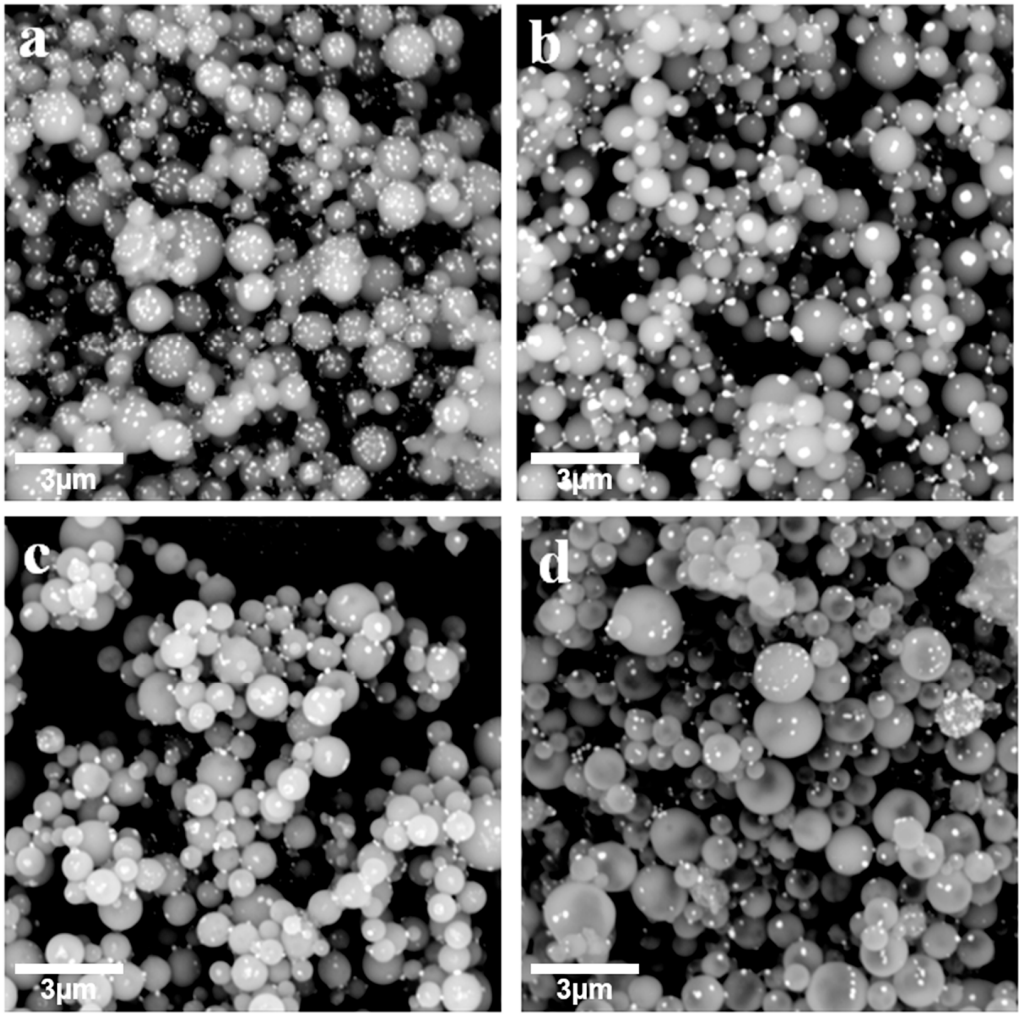

Figure 2. SEM photos of as-synthesized $LiFePO_4$ precursor powder at spray drying temperature of (**a**) 200 °C, (**b**) 250 °C, (**c**) 300 °C and (**d**) 350 °C.

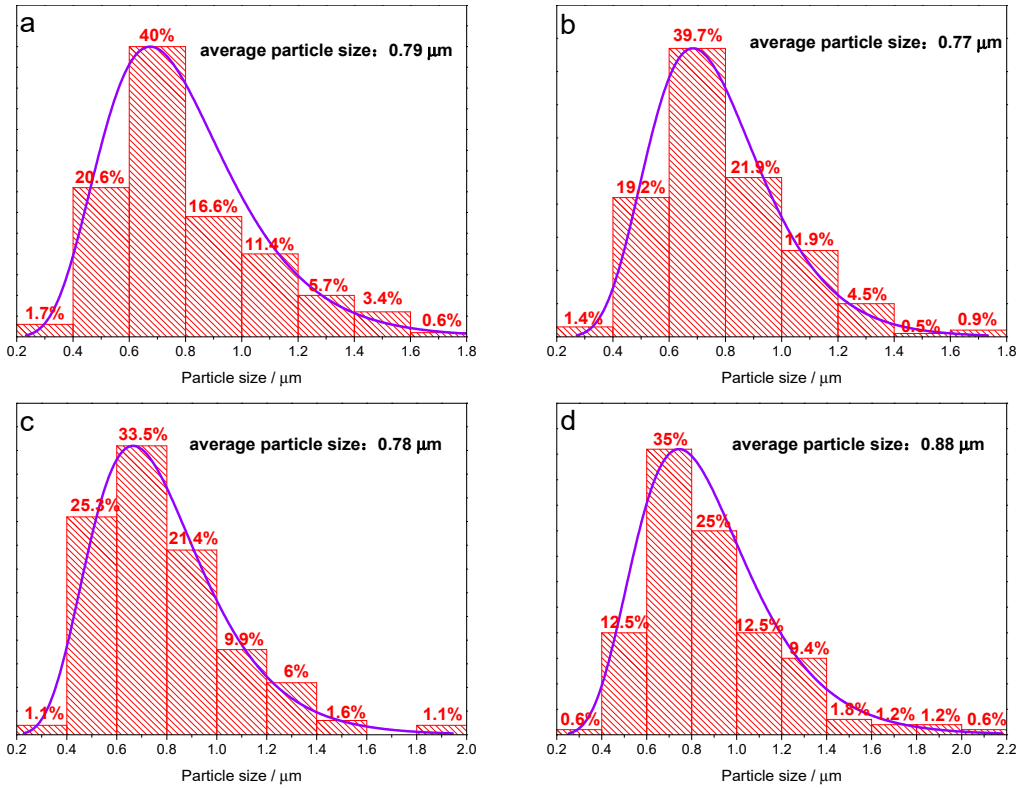

Figure 3. Particle size distribution of as-synthesized $LiFePO_4$ precursor powder at spray drying temperature of (**a**) 200 °C, (**b**) 250 °C, (**c**) 300 °C and (**d**) 350 °C.

As shown in Figure 4, the thermogravimetric analysis (TGA) was carried out for $LiFePO_4$ samples prepared at different spray drying temperatures. All samples exhibit very similar TGA curves, where the samples were heated from room temperature to 850 °C at a rate of 10 °C/min with an air flow of 70 mL/min. The weight loss below 310 °C can be attributed to the crystal water, which is about 0.36%. When the temperature rises to 310 °C, the $LiFePO_4$ samples began to be oxidized to $Li_3Fe_2(PO_4)_3$ and Fe_2O_3, thus the weight increases by 5.07%, theoretically, based on the following reaction formula [45,46]:

$$LiFePO_4 + \frac{1}{4}O_2 = \frac{1}{3}Li_3Fe_2(PO_4)_3 + \frac{1}{6}Fe_2O_3 \quad (1)$$

At about 580 °C, the carbon in the samples is oxidized into CO_2 with a weight loss. Therefore, the total weight has increased by 1.8%, and the carbon content in the sample should be 2.91%. The carbon comes from sucrose in the precursor solution, which is used to improve the conductivity of $LiFePO_4$. As we expected, the TGA result indicates that the $LiFePO_4$ sample has standard thermal stability in air.

As shown in Figure 5, the XRD patterns of all $LiFePO_4$ samples are consistent with that of olivine $LiFePO_4$ (PDF card number: 81-1173), indicating no impurity phase. All XRD data were analyzed by Rietveld refinement with General Structure Analysis System (GSAS) software [41], which is an important method to understand the crystal structure, cell parameters and other information of crystal materials. Figure 6a–d shows the refinement results calculated from Pnma phase group of $LiFePO_4$ collected at 200 °C, 250 °C, 300 °C and 350 °C during the spray drying process. The black line, red circle and blue line correspond to the observed pattern, the calculated diffraction pattern and the difference pattern, respectively. There are no sharp peaks at the Bragg position of the blue difference curve, indicating a very successful fit. In addition, the Rietveld refinement results provide excellent fits based on the Rwp, Rp and $\chi 2$ fitting factors, and they are concentrated in very small ranges of 1.3% to 1.5%, 1.1% to 1.2% and 1.1 to 1.3, respectively.

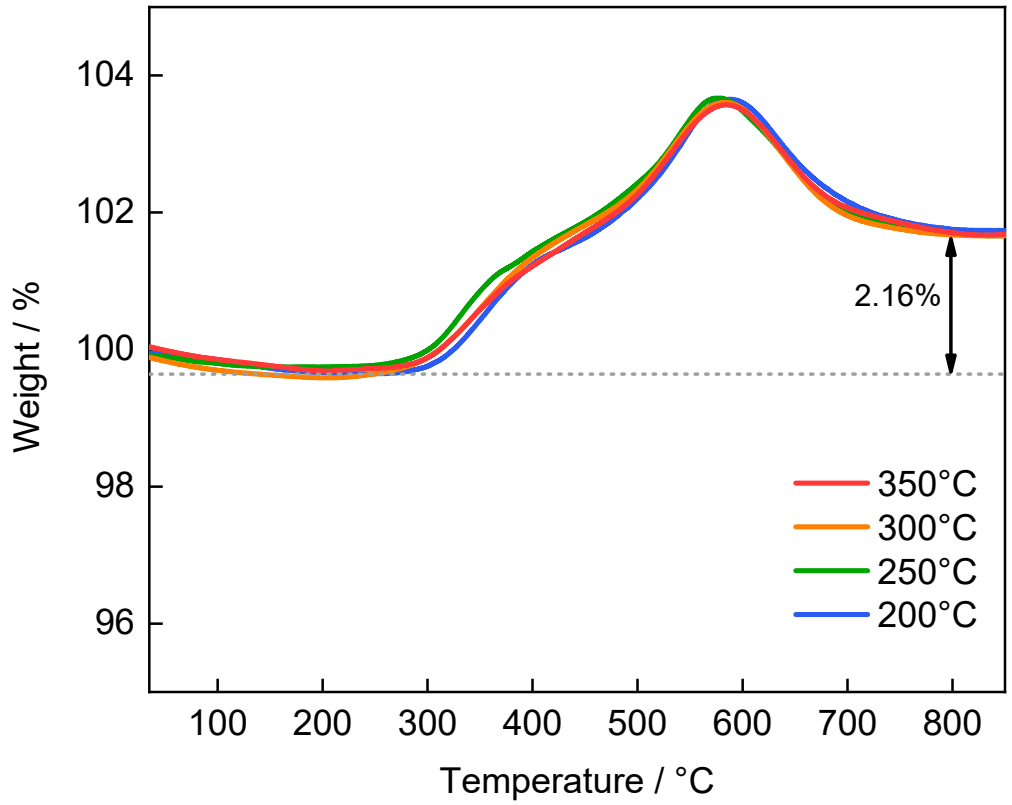

Figure 4. TGA curve of $LiFePO_4$ samples prepared at spray drying temperature of 200 °C, 250 °C, 300 °C and 350 °C.

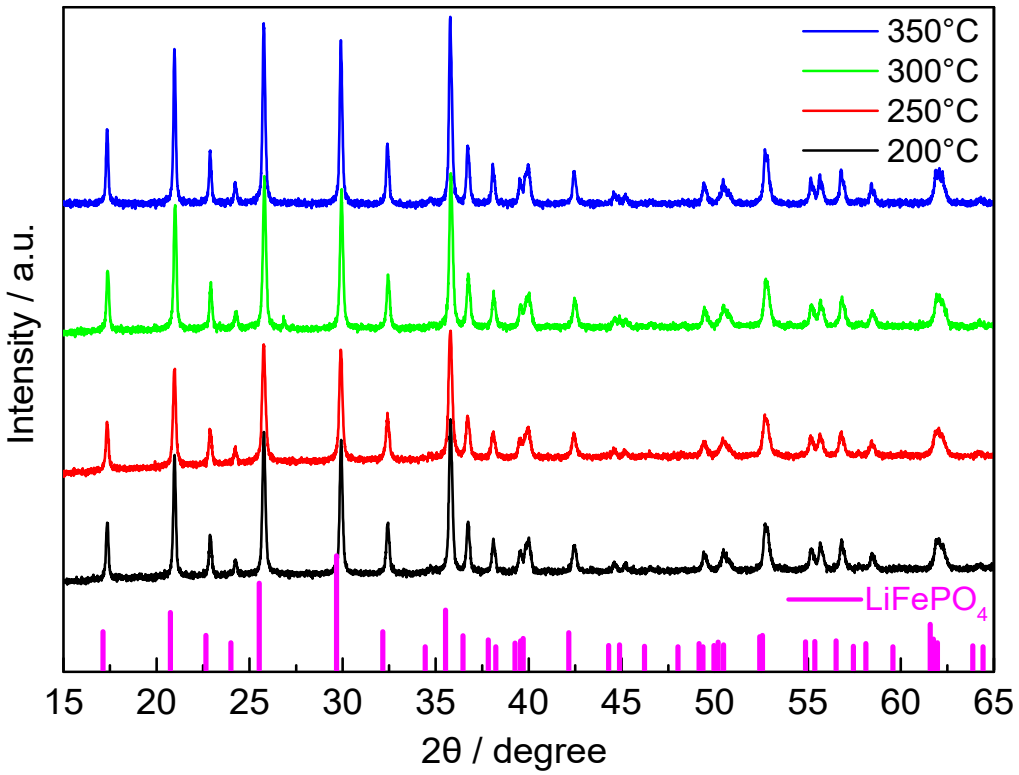

Figure 5. XRD patterns of $LiFePO_4$ samples prepared at spray drying temperature of 200 °C, 250 °C, 300 °C and 350 °C.

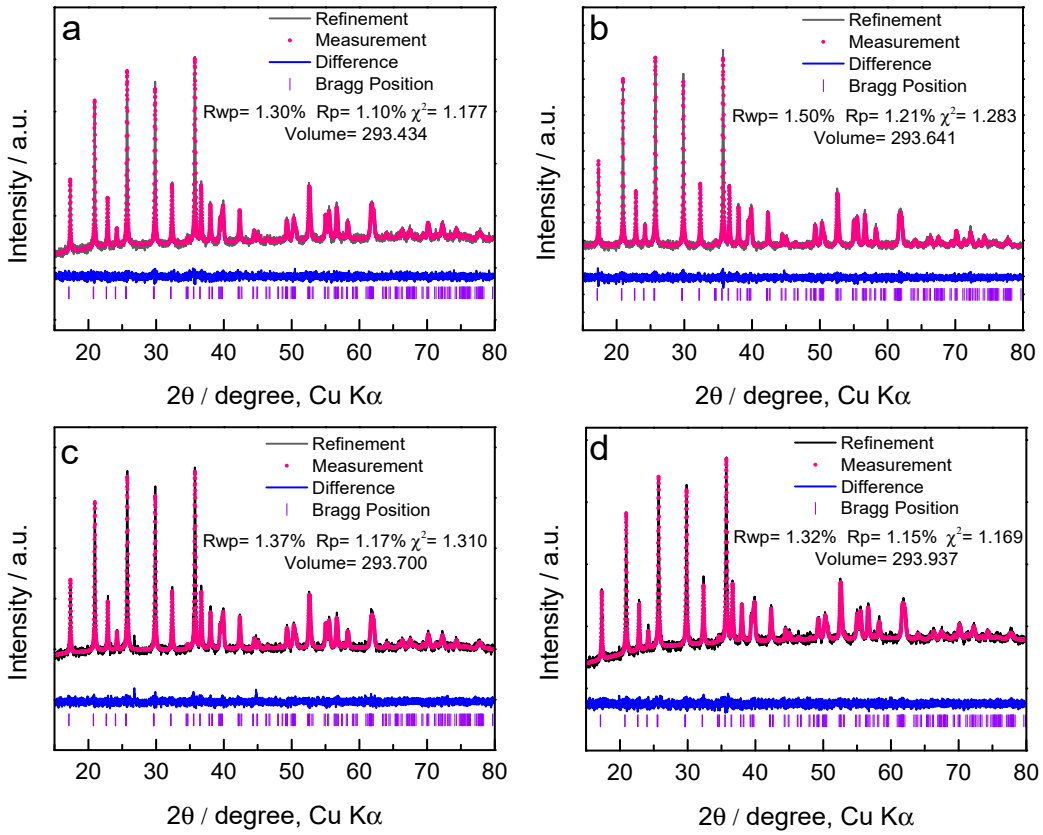

Figure 6. XRD spectra of $LiFePO_4$ samples prepared at spray drying temperature of (**a**) 200 °C, (**b**) 250 °C, (**c**) 300 °C and (**d**) 350 °C, as well as Rietveld refinement of Pnma. The black line, the red circle and the blue line correspond to the observed pattern, the calculated diffraction pattern and the difference pattern.

The cell volume of $LiFePO_4$ samples of 200 °C, 250 °C, 300 °C and 350 °C is 293.434 $Å^3$, 293.641 $Å^3$, 293.7 $Å^3$ and 293.937 $Å^3$, respectively. By increasing the spray drying temperature, the unit cell volume of $LiFePO_4$ increases gradually, which is caused by the disorder of crystal structure. When Fe^{2+} ions in M2 position move to M1 position to replace Li ions, this Li–Fe dislocation will destroy the most stable structure of $LiFePO_4$, resulting in distorted structure with larger cell volume. In fact, the Li–Fe dislocations are the most favorable defect in $LiFePO_4$ and have the lowest formation energy [47], in which the Fe^{2+} ions will expand the unit cell along a and c, due to having a larger size than Li^+ ions [48,49]. However, they barely affect the unit cell along b, for there is more channel space to accommodate the Fe^{2+} ions. Consequently, the disordered Fe^{2+} ions will block Li^+ ions in the (101) channels that are for Li^+ ions deintercalation in $LiFePO_4$ [50,51]. Therefore, the Li–Fe dislocations should be dependent on the spray drying temperature.

In Figure 7, the peaks of FTIR spectra locate at 469, 549, 640, 966, and 1055 cm^{-1} for $LiFePO_4$ samples [52]. The peak at 463 cm^{-1} is due to the bending harmonics of O–P–O and O=P–O groups. The peaks located at 547 and 638 cm^{-1} are assigned to the stretching vibrations of the P–O–P group and the peak at 966 cm^{-1} corresponds to P–O–P bending modes. The band observed at 1043 cm^{-1} corresponds to vibration of $(PO_4)^{3-}$ link metal ions [53,54]. As the spray drying temperature increases, the blue shift of the peak at 966 cm^{-1} is correlated to the Li–Fe antisite defects [55,56], thus suggesting that the increase in spray drying temperature will increase dislocations of $LiFePO_4$. This is consistent with the result of the XRD refinement.

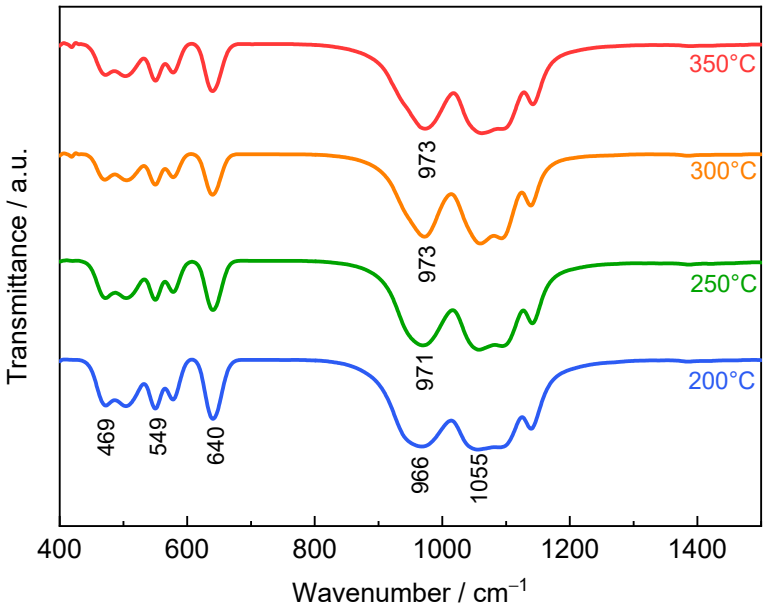

Figure 7. FTIR spectra of $LiFePO_4$ samples prepared at spray drying temperature of 200 °C, 250 °C, 300 °C and 350 °C.

As shown in Figure 8a,c,e,g, $LiFePO_4$ samples prepared at spray drying temperatures of 200 °C, 250 °C, 300 °C and 350 °C have specific capacity of 161.15 mAh/g, 157.4 mAh/g, 155 mAh/g and 151 mAh/g, which decreases as the spray drying temperature increases from 200 °C to 350 °C. Their memory effect is enhanced after increasing the spray drying temperature, as the ΔU, the potential gap between memory-releasing cycle and memory-writing cycle, is 1.3 mV, 1.7 mV, 2.5 mV and 2.9 mV for 200 °C, 250 °C, 300 °C and 350 °C, respectively. Combining the results of FTIR and XRD refinement, the reason that the memory effect of $LiFePO_4$ increases with the spray drying temperature can be attributed to the increment of Li–Fe dislocations. In olivine $LiFePO_4$, Li–Fe dislocations can block the [010] channel of Li-ion migration [57,58], which was proved by advanced electron microscopy, neutron diffraction (or X-ray diffraction) and theoretical calculations [39,51,59], so the lower specific capacity of $LiFePO_4$ may be due to the increased Li–Fe dislocations, consistent with previously reports [25,60].

Except for the spray drying temperature, the memory effect of $LiFePO_4$ has been studied by controlling the relaxation time, the voltage overshooting, the sintering temperature, the particle size, the lithium excess, etc., in previous investigations. As to the relaxation time [37], the memory effect is significantly dependent on the relaxation time after phase transition, and a rest of 20 h was added into the memory writing process to enhance the memory effect, while we also observed the evident memory effect without a rest in the memory-writing cycle for this work. As to the voltage overshooting [37], the voltage bump of memory effect is considered as a delayed voltage overshooting, which is overlaid at the edge of stepped (dis)charging plateau, while the voltage bump is small compared with the voltage step owing to the low sintering temperature of 650 °C in this work. As to the sintering temperature [37], the memory effect is noticeable for the high temperature of 800 °C, especially for the voltage bump at the step edge, while the increasing of spray drying temperature strengthened the memory effect of $LiFePO_4$ in this work, so the high temperature in the synthesis process can lead to the strong memory effect. As to the particle size [36], the memory effect of micro $LiFePO_4$ is stronger than that of nano $LiFePO_4$, which can be attributed to the fact that the phase transition of micro particles is slower than that of nano particles, while the different spray drying temperature can also affect the particle size in this work, and the $LiFePO_4$ sample prepared at a high spray drying temperature of 350 °C exhibits an evident memory effect, consistent with the previous work. As to the lithium excess [39], Kyu et al. studied the effect of excessive Li on the memory effect of $LiFePO_4$, and the results showed that in the case of excessive Li, the memory

effect of $LiFePO_4$ was significantly reduced, due to the presence of Li_{Fe} and the absence of Fe_{Li} in lithium-excess olivine $LiFePO_4$; similarly, the spray drying temperature affects the memory effect of $LiFePO_4$ through changing the Li–Fe anti-site defects in this work.

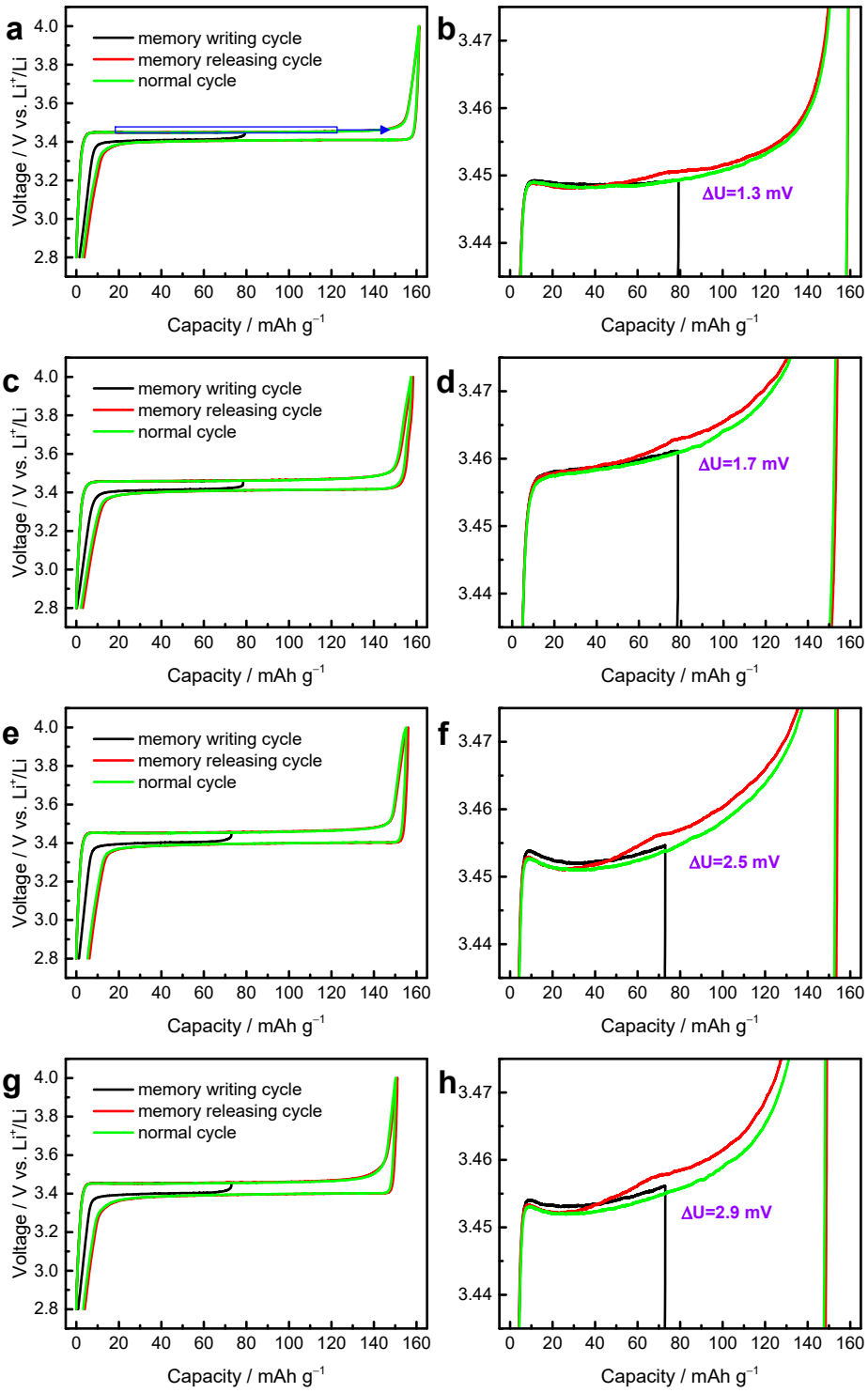

Figure 8. Determination of the memory effect during charging for $LiFePO_4$. For memory effect during charging, the memory-writing cycle was a half-charge from 2.8 V and a discharge to 2.8 V (black); the memory-releasing cycle (red) and normal cycle (green) were a full charge–discharge from 2.8 V to 4.0 V. The memory effect is shown for $LiFePO_4$ samples prepared at spray drying temperatures of (**a**,**b**) 200 °C, (**c**,**d**) 250 °C, (**e**,**f**) 300 °C and (**g**,**h**) 350 °C during charging, as well as (**b**,**d**,**f**,**h**) enlarged view of (**a**,**c**,**e**,**g**), respectively. Here, the current rate was 0.1C.

4. Conclusions

In this work, we set up a convenient home-made spray drying piece of equipment, prepared a series of $LiFePO_4$ with different spray drying temperatures, and studied their electrochemical performance in lithium-ion batteries. As the spray drying temperature varies from 200 °C to 350 °C, the memory effect of $LiFePO_4$ was enhanced from 1.3 mV to 2.9 mV, and the specific capacity was reduced from 161 mAh/g to 151 mAh/g. XRD refinement and FTIR analysis show that the Li–Fe dislocations increase with the spray drying temperature in $LiFePO_4$ samples. The defect of Li–Fe anti-site blocked some [010] channels of $LiFePO_4$ structure to retard the Li-ion migration, resulting in the memory effect. Our results show that the spray drying temperature has a significant impact on the memory effect and specific capacity of electrode materials, which can be adopted to improve and optimize electrode materials.

Author Contributions: Methodology, D.L.; software, X.G.; investigation, X.G., T.L.; writing—original draft preparation, X.G., T.L.; writing—review and editing, T.L., X.G., D.L., Y.C.; supervision, D.L.; funding acquisition, Y.C. All authors have read and agreed to the published version of the manuscript.

Funding: This research was funded by Key Research and Development Project of Hainan Province (ZDYF2019012 and ZDYF2020028), National Natural Science Foundation of China (21603048 and 52062012), the Innovation Team of Universities of Guangdong Province (2020KCXTD011), the Engineering Research Center of Universities of Guangdong Province (2019GCZX002), and the Guangdong Key Laboratory for Hydrogen Energy Technologies (2018B030322005).

Institutional Review Board Statement: Not applicable.

Informed Consent Statement: Not applicable.

Data Availability Statement: The data presented in this study are available on request from the corresponding author after obtaining permission from an authorized person.

Conflicts of Interest: The authors declare no conflict of interest.

References

1. Yang, Z.; Zhang, J.; Kintner-Meyer, M.C.W.; Lu, X.; Choi, D.; Lemmon, J.P.; Liu, J. Electrochemical Energy Storage for Green Grid. *Chem. Rev.* **2011**, *111*, 3577–3613. [CrossRef]
2. Liu, C.; Li, F.; Ma, L.-P.; Cheng, H.-M. Advanced Materials for Energy Storage. *Adv. Mater.* **2010**, *22*, E28–E62. [CrossRef] [PubMed]
3. Song, H.-K.; Lee, K.T.; Kim, M.G.; Nazar, L.F.; Cho, J. Recent Progress in Nanostructured Cathode Materials for Lithium Secondary Batteries. *Adv. Funct. Mater.* **2010**, *20*, 3818–3834. [CrossRef]
4. Hawkins, T.R.; Gausen, O.M.; Strømman, A.H. Environmental impacts of hybrid and electric vehicles—A review. *Int. J. Life Cycle Assess.* **2012**, *17*, 997–1014. [CrossRef]
5. Fergus, J.W. Recent developments in cathode materials for lithium ion batteries. *J. Power Sources* **2010**, *195*, 939–954. [CrossRef]
6. Marom, R.; Amalraj, S.F.; Leifer, N.; Jacob, D.; Aurbach, D. A review of advanced and practical lithium battery materials. *J. Mater. Chem.* **2011**, *21*, 9938–9954. [CrossRef]
7. Lu, L.; Han, X.; Li, J.; Hua, J.; Ouyang, M. A review on the key issues for lithium-ion battery management in electric vehicles. *J. Power Sources* **2013**, *226*, 272–288. [CrossRef]
8. Whittingham, M.S. Lithium Batteries and Cathode Materials. *Chem. Rev.* **2004**, *104*, 4271–4302. [CrossRef]
9. Padhi, A.K.; NanjundaSwamy, K.S.; Goodenough, J.B. Phospho-olivines as Positive-Electrode Materials for Rechargeable Lithium Batteries. *J. Electrochem. Soc.* **1997**, *144*, 1188–1194. [CrossRef]
10. Takahashi, M. Reaction behavior of LiFePO4 as a cathode material for rechargeable lithium batteries. *Solid State Ionics* **2002**, *148*, 283–289. [CrossRef]
11. Armand, M.; Tarascon, J.M. Building better batteries. *Nature* **2008**, *451*, 652–657. [CrossRef] [PubMed]
12. Kang, B.; Ceder, G. Battery materials for ultrafast charging and discharging. *Nat. Cell Biol.* **2009**, *458*, 190–193. [CrossRef] [PubMed]
13. Wang, J.; Sun, X. Olivine LiFePO4: The remaining challenges for future energy storage. *Energy Environ. Sci.* **2015**, *8*, 1110–1138. [CrossRef]
14. Chiu, K.-F.; Chen, C.-L. Electrochemical performance of magnetron sputter deposited LiFePO4-Ag composite thin film cathodes. *Surf. Coatings Technol.* **2010**, *205*, 1642–1646. [CrossRef]
15. Swain, P.; Viji, M.; Mocherla, P.S.; Sudakar, C. Carbon coating on the current collector and LiFePO4 nanoparticles—Influence of sp and sp-like disordered carbon on the electrochemical properties. *J. Power Sources* **2015**, *293*, 613–625. [CrossRef]

16. He, R.; Liu, Z.; Zhang, L.; Guo, R.; Yang, S. Electrochemical properties of V and Ti co-doping Li1.02FePO4/C material prepared by solid-state synthesis route. *J. Alloys Compd.* **2016**, *662*, 461–466. [CrossRef]
17. Yuan, H.; Wang, X.; Wu, Q.; Shu, H.; Yang, X. Effects of Ni and Mn doping on physicochemical and electrochemical performances of LiFePO4/C. *J. Alloys Compd.* **2016**, *675*, 187–194. [CrossRef]
18. Liu, Y.; Zhang, M.; Li, Y.; Hu, Y.; Zhu, M.; Jin, H.; Li, W. Nano-sized LiFePO4/C composite with core-shell structure as cathode material for lithium ion battery. *Electrochim. Acta* **2015**, *176*, 689–693. [CrossRef]
19. Bai, N.; Xiang, K.; Zhou, W.; Lu, H.; Zhao, X.; Chen, H. LiFePO4/carbon nanowires with 3D nano-network structure as potential high performance cathode for lithium ion batteries. *Electrochim. Acta* **2016**, *191*, 23–28. [CrossRef]
20. Zhang, Y.; Huo, Q.-Y.; Du, P.-P.; Wang, L.-Z.; Zhang, A.-Q.; Song, Y.-H.; Lv, Y.; Li, G.-Y. Advances in new cathode material LiFePO4 for lithium-ion batteries. *Synth. Met.* **2012**, *162*, 1315–1326. [CrossRef]
21. Kang, H.-C.; Jun, D.-K.; Jin, B.; Jin, E.M.; Park, K.-H.; Gu, H.-B.; Kim, K.-W. Optimized solid-state synthesis of LiFePO4 cathode materials using ball-milling. *J. Power Sources* **2008**, *179*, 340–346. [CrossRef]
22. Park, K.; Kang, K.; Lee, S.; Kim, G.; Park, Y.; Kim, H. Synthesis of LiFePO4 with fine particle by co-precipitation method. *Mater. Res. Bull.* **2004**, *39*, 1803–1810. [CrossRef]
23. Park, K.; Son, J.; Chung, H.; Kim, S.; Lee, C.; Kim, H. Synthesis of LiFePO4 by co-precipitation and microwave heating. *Electrochem. Commun.* **2003**, *5*, 839–842. [CrossRef]
24. Jugović, D.; Uskoković, D. A review of recent developments in the synthesis procedures of lithium iron phosphate powders. *J. Power Sources* **2009**, *190*, 538–544. [CrossRef]
25. Liu, J.; Jiang, R.; Wang, X.; Huang, T.; Yu, A. The defect chemistry of LiFePO4 prepared by hydrothermal method at different pH values. *J. Power Sources* **2009**, *194*, 536–540. [CrossRef]
26. Gao, F.; Tang, Z.; Xue, J. Preparation and characterization of nano-particle LiFePO4 and LiFePO4/C by spray-drying and post-annealing method. *Electrochim. Acta* **2007**, *53*, 1939–1944. [CrossRef]
27. Konarova, M.; Taniguchi, I. Preparation of LiFePO4/C composite powders by ultrasonic spray pyrolysis followed by heat treatment and their electrochemical properties. *Mater. Res. Bull.* **2008**, *43*, 3305–3317. [CrossRef]
28. Yang, M.-R.; Teng, T.-H.; Wu, S.-H. LiFePO4/carbon cathode materials prepared by ultrasonic spray pyrolysis. *J. Power Sources* **2006**, *159*, 307–311. [CrossRef]
29. Teng, T.-H.; Yang, M.-R.; Wu, S.-H.; Chiang, Y.-P. Electrochemical properties of LiFe0.9Mg0.1PO4 / carbon cathode materials prepared by ultrasonic spray pyrolysis. *Solid State Commun.* **2007**, *142*, 389–392. [CrossRef]
30. Jung, D.S.; Hwang, T.H.; Bin Park, S.; Choi, J.W. Spray Drying Method for Large-Scale and High-Performance Silicon Negative Electrodes in Li-Ion Batteries. *Nano Lett.* **2013**, *13*, 2092–2097. [CrossRef]
31. Wan, C.; Wu, M.; Wu, D. Synthesis of spherical LiMn2O4 cathode material by dynamic sintering of spray-dried precursors. *Powder Technol.* **2010**, *199*, 154–158. [CrossRef]
32. Sasaki, T.; Ukyo, Y.; Novák, P. Memory effect in a lithium-ion battery. *Nat. Mater.* **2013**, *12*, 569–575. [CrossRef] [PubMed]
33. Madej, E.; La Mantia, F.; Schuhmann, W.; Ventosa, E. Impact of the Specific Surface Area on the Memory Effect in Li-Ion Batteries: The Case of Anatase TiO2. *Adv. Energy Mater.* **2014**, *4*, 1400829. [CrossRef]
34. Li, D.; Sun, Y.; Liu, X.; Peng, R.; Zhou, H. Doping-induced memory effect in Li-ion batteries: The case of Al-doped Li4Ti5O12. *Chem. Sci.* **2015**, *6*, 4066–4070. [CrossRef] [PubMed]
35. Ulldemolins, M.; LE Cras, F.; Pecquenard, B. Memory effect highlighting in silicon anodes for high energy density lithium-ion batteries. *Electrochem. Commun.* **2013**, *27*, 22–25. [CrossRef]
36. Guo, X.; Song, B.; Yu, G.; Wu, X.; Feng, X.; Li, D.; Chen, Y. Size-Dependent Memory Effect of the LiFePO4 Electrode in Li-Ion Batteries. *ACS Appl. Mater. Interfaces* **2018**, *10*, 41407–41414. [CrossRef] [PubMed]
37. Jia, J.; Tan, C.; Liu, M.; Li, D.; Chen, Y. Relaxation-Induced Memory Effect of LiFePO4 Electrodes in Li-Ion Batteries. *ACS Appl. Mater. Interfaces* **2017**, *9*, 24561–24567. [CrossRef]
38. Shi, W.; Wang, J.; Zheng, J.; Jiang, J.; Viswanathan, V.; Zhang, J.-G. Influence of memory effect on the state-of-charge estimation of large-format Li-ion batteries based on LiFePO4 cathode. *J. Power Sources* **2016**, *312*, 55–59. [CrossRef]
39. Park, K.-Y.; Park, I.; Kim, H.; Yoon, G.; Gwon, H.; Cho, Y.; Yun, Y.S.; Kim, J.-J.; Lee, S.; Ahn, D.; et al. Lithium-excess olivine electrode for lithium rechargeable batteries. *Energy Environ. Sci.* **2016**, *9*, 2902–2915. [CrossRef]
40. Ventosa, E.; Löffler, T.; La Mantia, F.; Schuhmann, W. Understanding memory effects in Li-ion batteries: Evidence of a kinetic origin in TiO 2 upon hydrogen annealing. *Chem. Commun.* **2016**, *52*, 11524–11526. [CrossRef]
41. Toby, B.H. EXPGUI, a graphical user interface forGSAS. *J. Appl. Crystallogr.* **2001**, *34*, 210–213. [CrossRef]
42. Yu, F.; Zhang, J.; Yang, Y.; Song, G. Porous micro-spherical aggregates of LiFePO4/C nanocomposites: A novel and simple template-free concept and synthesis via sol–gel-spray drying method. *J. Power Sources* **2010**, *195*, 6873–6878. [CrossRef]
43. Yang, G.; Jiang, C.; He, X.; Ying, J.; Gao, J.; Wan, C. Synthesis of Size-controllable LiFePO4/C Cathode Material by Controlled Crystallization. *J. New Mater. Electrochem. Syst.* **2012**, *15*, 75–78. [CrossRef]
44. Liu, T.; Zhao, L.; Wang, D.; Zhu, J.; Wang, B.; Guo, C. Carbon-coated single-crystalline LiFePO4 nanocomposites for high-power Li-ion batteries: The impact of minimization of the precursor particle size. *RSC Adv.* **2014**, *4*, 10067–10075. [CrossRef]
45. Yu, J.; Hu, J.; Li, J. One-pot synthesis and electrochemical reactivity of carbon coated LiFePO4 spindles. *Appl. Surf. Sci.* **2012**, *263*, 277–283. [CrossRef]

46. Wang, X.; Feng, Z.; Huang, J.; Deng, W.; Li, X.; Zhang, H.; Wen, Z. Graphene-decorated carbon-coated LiFePO4 nanospheres as a high-performance cathode material for lithium-ion batteries. *Carbon* **2018**, *127*, 149–157. [CrossRef]
47. Fisher, C.A.J.; Prieto, V.M.H.; Islam, M.S. Lithium Battery Materials LiMPO4 (M = Mn, Fe, Co, and Ni): Insights into Defect Association, Transport Mechanisms, and Doping Behavior. *Chem. Mater.* **2008**, *20*, 5907–5915. [CrossRef]
48. Wang, L.; He, X.; Sun, W.; Wang, J.; Li, Y.; Fan, S. Crystal Orientation Tuning of LiFePO4 Nanoplates for High Rate Lithium Battery Cathode Materials. *Nano Lett.* **2012**, *12*, 5632–5636. [CrossRef] [PubMed]
49. Jensen, K.M.Ø.; Christensen, M.; Gunnlaugsson, H.P.; Lock, N.; Bøjesen, E.D.; Proffen, T.; Iversen, B.B. Defects in Hydrothermally Synthesized LiFePO4and LiFe1-xMnxPO4Cathode Materials. *Chem. Mater.* **2013**, *25*, 2282–2290. [CrossRef]
50. Zou, Y.; Chen, S.; Yang, X.; Ma, N.; Xia, Y.; Yang, D.; Guo, S. Suppressing Fe-Li Antisite Defects in LiFePO4/Carbon Hybrid Microtube to Enhance the Lithium Ion Storage. *Adv. Energy Mater.* **2016**, *6*, 1601549. [CrossRef]
51. Liu, H.; Choe, M.-J.; Enrique, R.A.; Orvañanos, B.; Zhou, L.; Liu, T.; Thornton, K.; Grey, C.P. Effects of Antisite Defects on Li Diffusion in LiFePO4 Revealed by Li Isotope Exchange. *J. Phys. Chem. C* **2017**, *121*, 12025–12036. [CrossRef]
52. Sundarayya, Y.; Swamy, K.K.; Sunandana, C. Oxalate based non-aqueous sol–gel synthesis of phase pure sub-micron LiFePO4. *Mater. Res. Bull.* **2007**, *42*, 1942–1948. [CrossRef]
53. Lu, Y.; Shi, J.; Guo, Z.; Tong, Q.; Huang, W.; Li, B. Synthesis of LiFe1−xNixPO4/C composites and their electrochemical performance. *J. Power Sources* **2009**, *194*, 786–793. [CrossRef]
54. Shu, H.; Wang, X.; Wu, Q.; Hu, B.; Yang, X.; Wei, Q.; Liang, Q.; Bai, Y.; Zhou, M.; Wu, C.; et al. Improved electrochemical performance of LiFePO4/C cathode via Ni and Mn co-doping for lithium-ion batteries. *J. Power Sources* **2013**, *237*, 149–155. [CrossRef]
55. Radhamani, A.; Karthik, C.; Ubic, R.; Rao, M.R.; Sudakar, C. Suppression of antisite defects in fluorine-doped LiFePO4. *Scr. Mater.* **2013**, *69*, 96–99. [CrossRef]
56. Qin, X.; Wang, J.; Xie, J.; Li, F.; Wen, L.; Wang, X. Hydrothermally synthesized LiFePO4 crystals with enhanced electrochemical properties: Simultaneous suppression of crystal growth along [010] and antisite defect formation. *Phys. Chem. Chem. Phys.* **2012**, *14*, 2669–2677. [CrossRef] [PubMed]
57. Nishimura, S.-I.; Kobayashi, G.; Ohoyama, K.; Kanno, R.; Yashima, M.; Yamada, A. Experimental visualization of lithium diffusion in LixFePO4. *Nat. Mater.* **2008**, *7*, 707–711. [CrossRef]
58. Malik, R.; Burch, D.; Bazant, M.; Ceder, G. Particle Size Dependence of the Ionic Diffusivity. *Nano Lett.* **2010**, *10*, 4123–4127. [CrossRef] [PubMed]
59. Hu, J.; Xiao, Y.; Tang, H.; Wang, H.; Wang, Z.; Liu, C.; Zeng, H.; Huang, Q.; Ren, Y.; Wang, C.; et al. Tuning Li-Ion Diffusion in α-LiMn1–xFexPO4 Nanocrystals by Antisite Defects and Embedded β-Phase for Advanced Li-Ion Batteries. *Nano Lett.* **2017**, *17*, 4934–4940. [CrossRef] [PubMed]
60. Chen, J.; Graetz, J. Study of Antisite Defects in Hydrothermally Prepared LiFePO4 by in Situ X-ray Diffraction. *ACS Appl. Mater. Interfaces* **2011**, *3*, 1380–1384. [CrossRef] [PubMed]